Stem Cell Reports
Article

ISSCR

OPEN ACCESS

Exosomes as Critical Agents of Cardiac Regeneration Triggered by Cell Therapy

Ahmed Gamal-Eldin Ibrahim,[1] Ke Cheng,[1] and Eduardo Marbán[1,*]
[1]Heart Institute, Cedars Sinai Medical Center, Los Angeles, CA 90048, USA
*Correspondence: eduardo.marban@cshs.org
http://dx.doi.org/10.1016/j.stemcr.2014.04.006

SUMMARY

The CADUCEUS trial of cardiosphere-derived cells (CDCs) has shown that it may be possible to regenerate injured heart muscle previously thought to be permanently scarred. The mechanisms of benefit are known to be indirect, but the mediators have yet to be identified. Here we pinpoint exosomes secreted by human CDCs as critical agents of regeneration and cardioprotection. CDC exosomes inhibit apoptosis and promote proliferation of cardiomyocytes, while enhancing angiogenesis. Injection of exosomes into injured mouse hearts recapitulates the regenerative and functional effects produced by CDC transplantation, whereas inhibition of exosome production by CDCs blocks those benefits. CDC exosomes contain a distinctive complement of microRNAs, with particular enrichment of miR-146a. Selective administration of a miR-146a mimic reproduces some (but not all) of the benefits of CDC exosomes. The findings identify exosomes as key mediators of CDC-induced regeneration, while highlighting the potential utility of exosomes as cell-free therapeutic candidates.

INTRODUCTION

Cardiosphere-derived cells (CDCs) stimulate regeneration, angiogenesis, and functional improvement in the infarcted myocardium (Kreke et al., 2012; Smith et al., 2007) by indirect mechanisms; most of the newly regenerated myocardium and vasculature are of endogenous origin (Chimenti et al., 2010), and the beneficial effects of CDCs persist long after the injected cells have been cleared (Malliaras et al., 2012). CDCs are rich biological factories that secrete many growth factors and cytokines (Stastna et al., 2010), but a possible role for exosomes has yet to be considered. Exosomes are lipid bilayer nanovesicles secreted by a variety of cells when multivesicular endosomes fuse with the plasma membrane (Denzer et al., 2000). Although first described decades ago (Pan and Johnstone, 1983; Pan et al., 1985), exosomes have attracted new interest sparked by the recognition that they play important roles in paracrine and autocrine signaling (Johnstone, 2005). Exosomes transfer proteins and RNA (Lugini et al., 2012), notably microRNAs (miRNAs) (Zhu and Fan, 2011), from cell to cell, rationalizing potential applications in clinical therapeutics (Arslan et al., 2013; Hergenreider et al., 2012; O'Loughlin et al., 2012). Here, we test the concept that CDC-secreted exosomes (CDC exosomes for short), and specifically the miRNAs transferred by these exosomes, mediate the protective effects of human CDCs in a murine model of myocardial infarction (MI).

RESULTS

CDC Exosomes Enhance Angiogenesis and Promote Cardiomyocyte Survival and Proliferation

Exosomes were isolated from serum-free media conditioned over 15 days by cultured human CDCs (or normal human dermal fibroblasts [NHDFs] as a therapeutically inert control) (Smith et al., 2007) (Figure S1 available online). By the end of the conditioning period, most of the CDCs remained alive despite the absence of regular media changes (Figures S1B and S1C). Purified exosome pellets were enriched in RNA (Figure 1A). We confirmed that the RNA resides within exosomes by exposing the pellet to RNase A in the presence of 5% triton (Figure 1B), with proteinase K added to dissociate protein complexes that may shield RNA (Arroyo et al., 2011). Mass spectrometry confirmed the presence of conserved exosomal biogenesis proteins (Figure 1C) including CD63, which we used (by prior convention; e.g., Singh et al., 2012b) to quantify exosome yield (Figure 1D). Transmission electron microscopy revealed most exosomes to be 30–90 nm in diameter, although smaller and larger particles were also present (Figures 1E and 1F), consistent with reports of exosomes derived from vascular cells (Hergenreider et al., 2012; Sahoo et al., 2011).

In vitro assays revealed major effects of CDC exosomes on angiogenesis, cardiomyocyte proliferation, and apoptosis. CDC exosomes, but not NHDF exosomes, promoted tube formation in human umbilical cord endothelial cells, indicative of enhanced angiogenesis (Figure 1G).

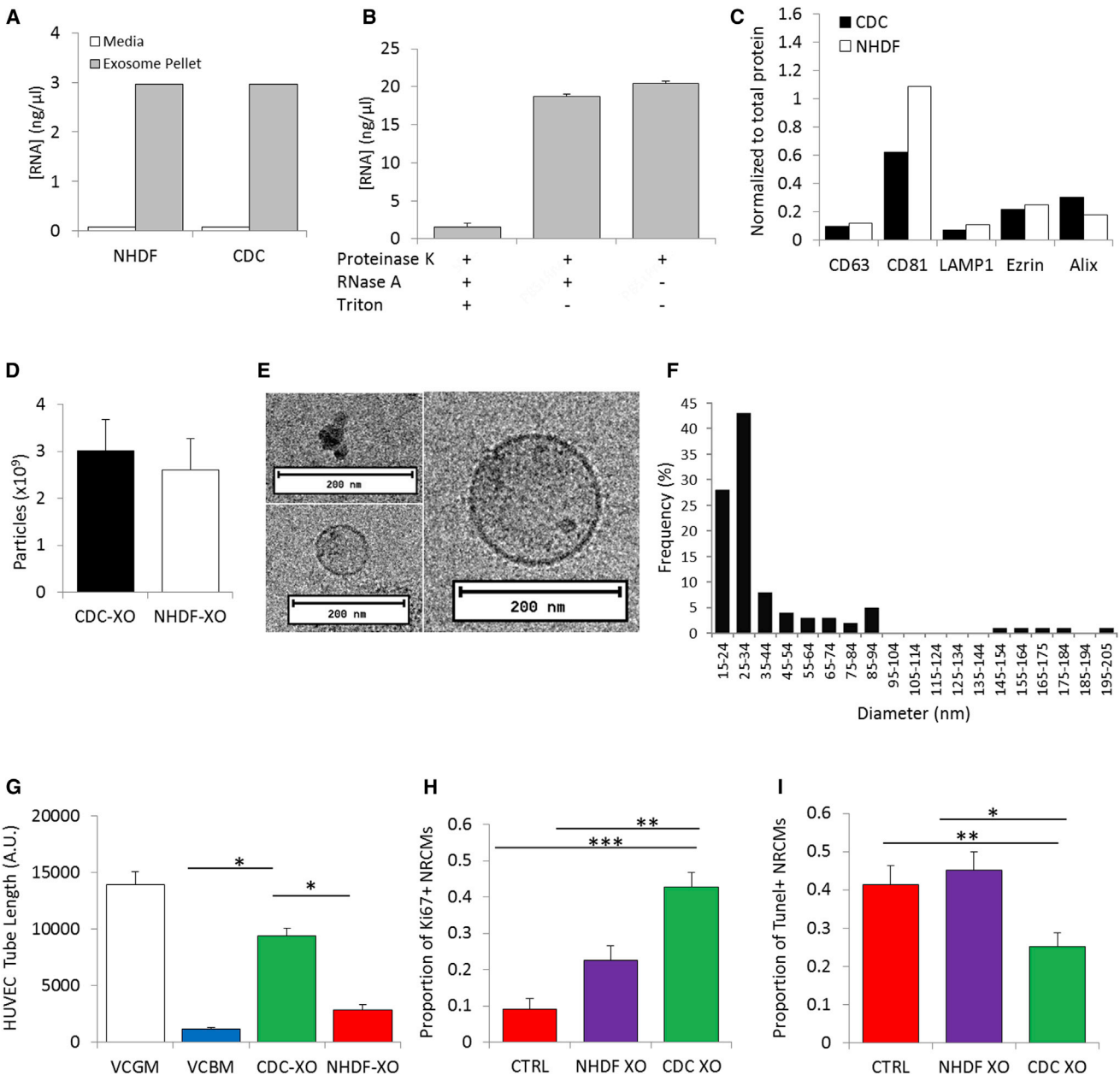

Figure 1. Characterization of CDC Exosomes

(A) RNA content measured in exosome pellets derived from CDCs and NHDFs compared to conditioned media from both samples.

(B) Exosomal RNA is protected from RNase degradation by the lipid bilayer membrane of exosomes. Exosome pellets were treated with RNase A in the presence or absence of triton to assess protection from RNase-mediated degradation. All samples were treated with proteinase K to dissociate complexes which might otherwise shield RNA (n = 4 technical replicates).

(C) CDC and NHDF exosomes express ubiquitous exosome markers as revealed by mass spectrometry.

(D) Exosome quantification from CDC- and NHDF-conditioned media based on expression of the conserved CD63 marker (n = 3 technical repeats).

(E) Exosomes isolated from CDCs visualized by transmission electron microscopy. Three populations (by size) are illustrated.

(F) Size distribution of exosomes derived from CDCs, measured from transmission electron microscopic images; n = 100 exosomes counted. CDC exosomes enhance angiogenesis and promote neonatal rat cardiomyocyte (NRCM) survival and proliferation in vitro.

(G) CDC exosomes stimulate angiogenesis compared to NHDF exosomes in a HUVEC angiogenesis assay. Quantification of angiogenesis assay by HUVEC tube length (vascular cell basal medium, VCGM as a negative control and vascular cell growth medium, VCGM, as a positive control). n = 3 technical replicates per group.

(legend continued on next page)

CDC-exosome-treated neonatal cardiomyocytes proliferated more than those exposed to NHDF exosomes or media only, as evidenced by higher proportions of Ki67-positive nuclei (Figure 1H). In addition, CDC-exosome-treated cardiomyocytes exhibited fewer terminal deoxynucleotidyltransferase nick end labeling (TUNEL)-positive nuclei (Figure 1I). Thus, CDC exosomes stimulate angiogenesis, promote cardiomyocyte proliferation, and decrease programmed cell death. These effects reproduce those of the parent CDCs (Kreke et al., 2012).

CDC Exosomes Improve Cardiac Function, Impart Structural Benefits, and Increase Viable Mass after MI

CDCs stimulate functional improvement and regeneration in the infarcted myocardium in both animals and humans (Kreke et al., 2012). To assess therapeutic efficacy in an established preclinical model, we induced acute MI in immunodeficient mice then injected CDC exosomes, NHDF exosomes, or serum-free media into the MI border zone (Cheng et al., 2014; Li et al., 2010; Smith et al., 2007). At 15 and 30 days after injection, global heart function was greater in animals injected with CDC exosomes compared with NHDF exosomes or media controls (Figure 2A). At the histological level, CDC-exosome-treated hearts exhibited decreased scar mass, increased viable mass, and increased infarcted wall thickness compared to NHDF exosome and media controls (Figures 2B–2E). Proinflammatory cytokine levels were also lower in CDC-exosome-treated hearts (Figure S2). In all these respects, CDC exosomes mimic the known benefits of CDCs themselves (Kreke et al., 2012).

The acute MI model, while used extensively to assess bioactivity, cannot distinguish cardioprotective effects from genuine regeneration (Malliaras et al., 2013). To make this distinction, we performed another set of experiments in which we injected exosomes 21 days after MI, when myocardial scar is well established (Virag and Murry, 2003). Three weeks later, hearts injected with CDC exosomes showed multiple structural and functional benefits: improved ejection fraction (Figure 2F; also improved fractional area change, Figure S3A), lower scar mass (representative images in Figure 2G and pooled data in Figure 2H), higher viable mass (Figure 2I), and thicker infarcted walls (Figure 2J). Moreover, hearts treated with CDC exosomes exhibited less chamber dilation (Figures S3B and S3C), smaller infarct circumference (Figure S3D), and diminished compensatory myocyte hypertrophy (Figures S3E and S3F) relative to the grossly distorted control hearts. The density of microvessels was increased (Figures 2K and S3G) and apoptotic cardiomyocyte nuclei were less frequent (Figures S3H and S3I) in CDC-exosome-treated hearts. The net growth of new myocardium in the setting of established scar fulfills the central criterion for therapeutic regeneration (Makkar et al., 2012); the improvement in function and the attenuation of adverse remodeling attest to the physiological significance of the tissue changes. We conclude that CDC exosomes indeed mediate genuine cardiac regeneration, while favoring angiogenesis and tissue preservation.

Inhibition of Exosome Secretion Attenuates CDC Benefit

If exosomes mediate the therapeutic effects of CDC transplantation, then inhibition of exosome secretion would logically be expected to block the benefits. To test this concept, we treated CDCs with GW4869, a reversible inhibitor of neutral sphingomyelinase that prevents exosome release (Kosaka et al., 2010; Trajkovic et al., 2008). Exposure to GW4869 blocked exosome production in a dose-dependent manner (Figure 3A), with complete suppression at 20 μM (a dose without apparent short-term cytotoxicity; e.g., no impairment of proliferation; Figure 3B). Suppression of exosome release abrogated the indirect benefits of CDCs in vitro because media conditioned by GW4869-treated CDCs did not enhance cardiomyocyte proliferation or attenuate apoptosis (Figures 3C and 3D). Spiroepoxide, a specific irreversible inhibitor of neutral sphingomyelinase (Trajkovic et al., 2008), mimicked the antiapoptotic effects of GW4869 on stressed cardiomyocytes (Figures S4A and S4B). In vivo, CDCs pretreated with GW4869 exerted no functional (Figure 3E) or structural (Figures 3F–3I) benefits in acute MI, in contrast to vehicle-only (DMSO) controls that conferred all the expected therapeutic effects of CDCs (Kreke et al., 2012). Thus, exosome secretion by CDCs is required for CDC-mediated benefits in vitro and in vivo.

CDC Exosomes Are Enriched in miR-146a, which Plays an Important Role in MI Pathology

To investigate the basis of the therapeutic benefit of CDC exosomes, we compared their miRNA repertoire to that of NHDF exosomes using a PCR microarray of the 88 best-defined miRNAs. The miRNA content of the two cell types differed dramatically. Forty-three miRNAs were differentially present in the two groups; among these, miR-146a was the most highly enriched in CDC exosomes

(H and I) CDC exosomes promote proliferation (Ki67-positive nuclei; H) and survival (inhibition of TUNEL-positive nuclei; I) in cultured neonatal cardiomyocytes; n = 4 technical replicates per group.
*p < 0.05, **p < 0.01, and ***p < 0.001 using one-way ANOVA (Tukey's post hoc test). Data are represented as mean and SEM. See also Figure S1.

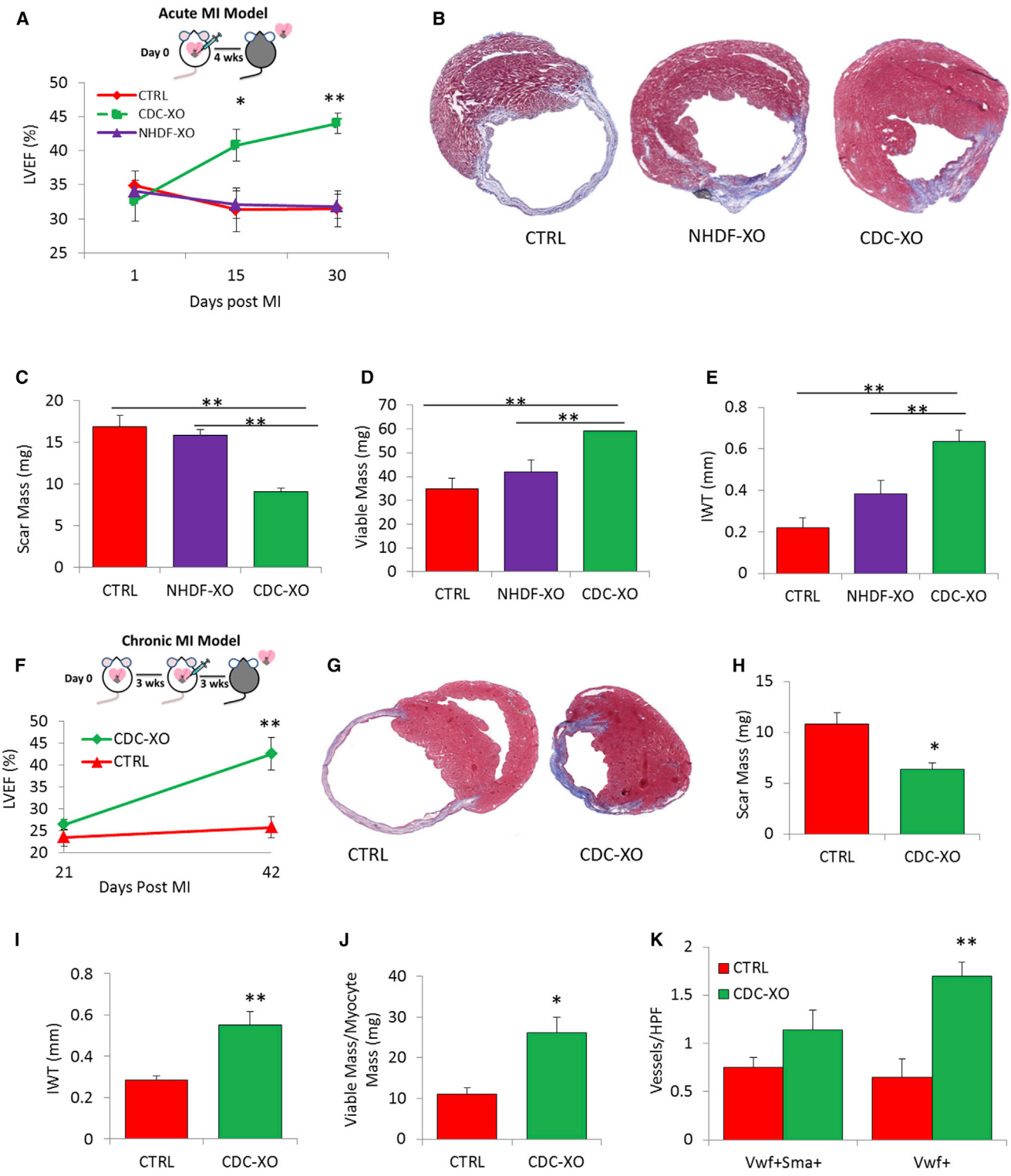

Figure 2. CDC Exosomes Produce Structural and Functional Benefits in Mouse Hearts after MI

(A) In the acute model, SCID Beige mice underwent MI and hearts were injected with CDC exosomes, NHDF exosomes, or vehicle (control). Animals (n = 8 animals per group) were echoed at days 1, 15, and 30 and were then sacrificed for histological analysis. CDC exosomes increase left ventricular ejection fraction (LVEF).

(legend continued on next page)

(262-fold higher than in NHDF exosomes; Figures 4A, 4B, and S5). Furthermore, miR-146a tissue levels were increased in post-MI hearts from animals injected with CDC exosomes relative to those injected with NHDF exosomes (Figure 4C), rendering plausible the idea that CDC exosomes might act via miR-146a transfer. Exposure of neonatal rat cardiomyocytes to a miR-146a mimic increased cardiomyocyte viability and protected against oxidant stress (Figures 4D and S6A). Whole-transcriptome microarrays revealed downregulation of *Irak1* and *Traf6*, two signaling mediators of the TLR-NFkB axis that are known targets of miR-146a (Huang et al., 2012; Wang et al., 2013) (Figure 4E). Ingenuity pathway analysis (Thomas and Bonchev, 2010) pointed to changes in pathways involved in cell survival, cell cycling, cellular organization, and morphology, all of which are relevant to ischemic injury (Figure S5D) and share links to the basal transcription factor Myc (Figure S5E).

To probe the biological role of miR-146a in myocardial injury, we induced acute MI in miR-146a knockout (146a KO) mice and compared them with wild-type mice of the same strain (WT), as well as 146a KO mice "rescued" by injection of a miR-146a mimic at the time of MI (146a KO-R). After MI, the 146a KO mice showed deeply impaired heart function and adverse remodeling compared to WT or 146a KO-R (Figures 4F and 4G). Histological analysis revealed significant increases in scar mass (Figure 4H) and decreases in infarct wall thickness in the 146a KO, but not in WT or 146a KO-R (Figure 4J). Viable mass was greatest in the 146a KO-R group (Figure 4I), perhaps indicating a supraphysiological effect of the injected miR-146a mimic. These findings point to a critical role of miR-146a in MI and give reason to suspect that miR-146a may mediate some of the therapeutic benefits of CDC exosomes.

miR-146a Leads to Thicker Infarct Wall Thickness and Increased Viable Tissue in a Mouse Model of MI

To investigate the contribution of miR-146a to the greater exosome effect, we developed miR-146a-deficient exosomes by transfecting CDCs with a miR-146a hairpin inhibitor (or a control hairpin) followed by media conditioning and exosome isolation. Successful knockdown of miR-146a was confirmed by qPCR on resultant exosomes and on NRVMs exposed to either control or miR-146a-depleted exosomes (Figures S6B and S6C). The antiapoptotic effect of CDC exosomes was evident by comparing TUNEL positivity in untreated NRVMs (left column, Figure 5A) to that in NRVMs treated with control CDC exosomes (right column, Figure 5A). Exosomes deficient in miR-146a conferred less protection from oxidant stress (middle column, Figure 5A) than did control CDC exosomes, but still significantly suppressed apoptosis. These data hint that miR-146a underlies some, but not all, of the beneficial effect of CDC exosomes. To further probe this question in vivo, we implemented the same MI models as in Figure 2 but injecting either a miR-146a mimic or a miRNA mimic control. Mice injected with miR-146a mimic during acute MI exhibited improved pump function (Figure 5B), decreased scar mass, and increased viable heart tissue (Figures 5C–5F). In the chronic MI model, where regeneration can be studied more rigorously, animals treated with miR-146a showed only minor, statistically insignificant functional improvement (Figures 5G and S7A). Furthermore, histological analysis showed no difference in scar mass (Figures 5H and 5I). However, hearts treated with miR-146a mimic did show increased viable tissue, thicker infarcted walls (Figures 5J and 5K), and less adverse remodeling than controls (Figures S7B–S7D). Evaluation of angiogenesis showed no significant differences between the two groups (Figures 5L and S7G). However, lower frequencies of cardiomyocyte apoptosis were observed in the miR-146a-injected hearts (Figures S7H and S7I), consistent with the in vitro data (Figure 5A). Thus, in the chronic MI model, miR-146a reproduces the cardiomyogenic and antiapoptotic effects, but not the remaining functional and structural benefits, of CDC exosomes (cf. Figures 2F–2J and S3A–S3C).

Exogenous miR-146a is known to suppress ischemia/reperfusion injury via targeting of Irak-1 and Traf6 (Cheng et al., 2013), both involved in the toll-like receptor (TLR) signaling pathway (Wang et al., 2013). TLR signaling underlying innate immunity plays a major role in the pathology of sterile inflammation, including MI (Arslan et al., 2010; Feng et al., 2008; Oyama et al., 2004; Singh et al.,

(B–E) Structural benefits of CDC exosomes. Representative Masson's trichrome-stained sections of hearts from each of the three groups (B) and pooled morphometric analysis (C–E; n = 3 hearts per group) reveal decreased scar and increased viable mass in hearts injected with CDC exosomes.

(F) In the chronic model, 3-month-old SCID Beige mice (n = 6 animals per group) underwent MI. Three weeks later, animals were injected intramyocardially with CDC exosomes or control. Functional measurements were taken 24 hr before injection (day 21) and 3 weeks later (day 42), after which animals were sacrificed for histological analysis.

(G–J) As in the acute MI model, CDC exosomes produce functional and structural benefits in mouse hearts (n = 4 hearts per group) in a model of chronic MI.

*p < 0.05, **p < 0.01, and ***p < 0.001 using one-way ANOVA with Tukey's post hoc test and two-tailed Student's t test. Data are represented as mean and SEM. See also Figures S2 and S3.

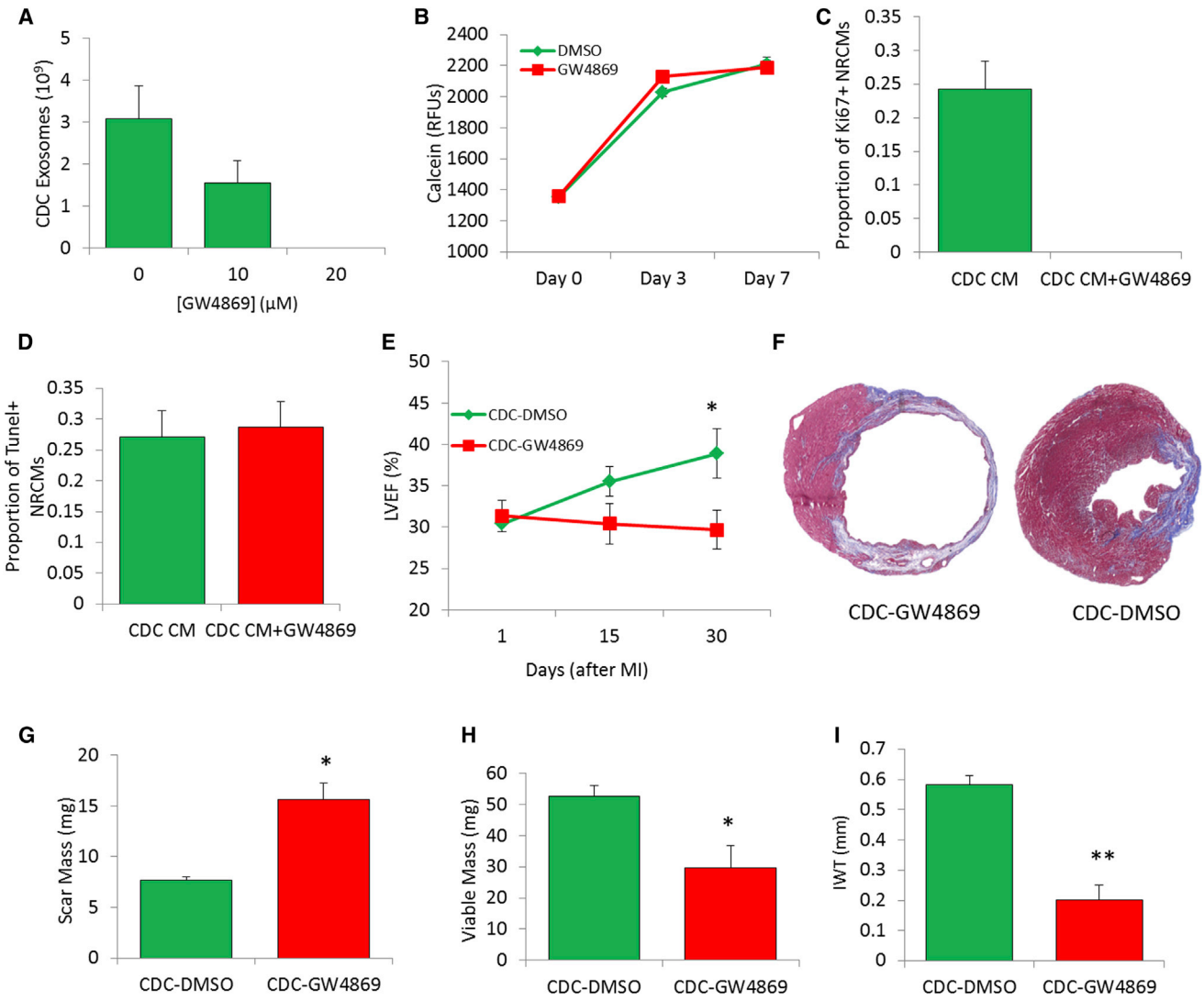

Figure 3. Exosome Inhibition Attenuates CDC-Mediated Benefits

(A) GW4869 inhibited exosome production in CDCs in a dose-dependent manner (n = 3 technical replicates).

(B) GW4869 does not affect CDC viability as shown by calcein assay of CDCs treated with GW4869 or its solvent DMSO (n = 4 technical replicates).

(C and D) Neonatal rat cardiomyocytes (NRCMs) were cultured on chamber slides and treated with media conditioned by CDCs exposed to either GW4869 or DMSO. NRCMs were then treated with culture media and after 5 days, slides were stained for Ki67 and TUNEL to assess proliferation and apoptosis (n = 4 technical replicates per group).

(E) Pooled data for left ventricular ejection fraction (n = 8 animals per group).

(F–I) Representative Masson's trichrome-stained heart sections from two groups (F) and pooled morphometric analysis (G–I; n = 4 hearts per group) reveal impairment of CDC-mediated benefit as evident in pooled data for scar mass, viable mass, and infarct wall thickness (IWT) in hearts injected with GW869-treated CDCs.

*p < 0.05 and **p < 0.01 using Student's t test. Data are represented as mean and SEM. See also Figure S4.

2012a). The CDC-exosome-mediated reductions of proinflammatory cytokines (Figure S2) and suppression of *Irak1* and *Traf6* by miR-146a (which is augmented in hearts injected with CDC exosomes; Figure 4C) are consistent with blunted TLR signaling. In addition, miR-146a suppresses NOX-4 (Vasa-Nicotera et al., 2011), which has been shown to impart oxidative stress and to potentiate cardiac injury (Infanger et al., 2010), and SMAD4, a member of the transforming growth factor β (TGF-β) profibrotic pathway (Liu et al., 2012). To confirm that these targets are indeed downregulated, we performed western blots on chronic MI hearts 7 days after treatment with miR-146a.

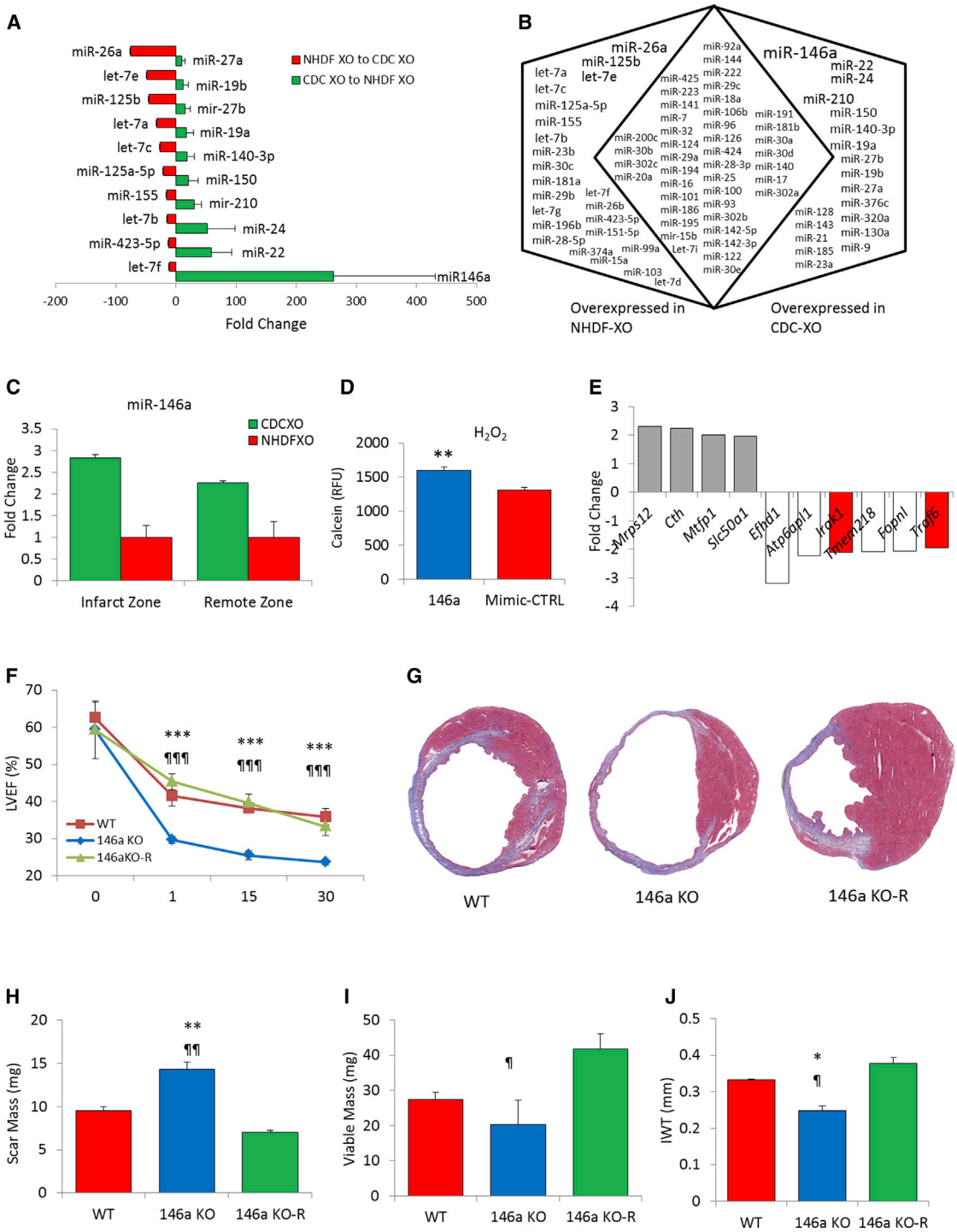

Figure 4. miR-146a Is Highly Enriched in CDC Exosomes and Confers Therapeutic Benefit In Vitro and In Vivo

(A) Fold changes of miRNA abundance in CDC exosomes compared to NHDF exosomes (n = 4 independent experiments). Total RNA (including miRNAs) was isolated from CDC exosomes and NHDF exosomes. qRT-PCR was performed on an miRNA array.

(B) Venn diagram showing the variable miRNA profile between CDC and NHDF exosomes. Font size reflects the magnitude of differential expression of each miRNA.

(C) Infarcted mouse hearts treated with CDC-derived exosomes have elevated levels of miR-146a compared to NHDF exosome-treated hearts (n = 2 animals per group, three technical replicates per group).

(legend continued on next page)

Indeed, all of the aforementioned targets were silenced in miR-146a-treated hearts compared to mimic control (Figures 6A and 6B). We also found lower levels of myeloperoxidase, a surrogate of neutrophil infiltration.

DISCUSSION

Cardiosphere-derived cells have been shown to induce therapeutic regeneration of the infarcted human heart. In a form of injury traditionally thought to be irreversible, CDCs led to shrinkage of scar and growth of new, functional myocardium (Makkar et al., 2012). Similar effects have been corroborated in animal models (Kreke et al., 2012; Makkar et al., 2012). Here, we show that exosomes reproduce CDC-induced therapeutic regeneration, and that inhibition of exosome production undermines the benefits of CDCs. Exosomes contain miRNAs, which have the ability to alter cell behavior through paracrine mechanisms (Figure 6B). Among these, we have identified miR-146a as being particularly enriched in CDC exosomes. When administered alone, miR-146a reproduces some, but not all, of the salient benefits of CDCs and of CDC exosomes (Figure 3). Likewise, miR-146a-depleted exosomes were still able to suppress cardiomyocyte apoptosis (Figure 5A), albeit more weakly than when miR-146a is present. Treating hearts with miR-146a in a chronic model of MI (after the scar is permanent) does reproduce the increase in viable mass that is the signature of therapeutic regeneration, but fails to mimic two key beneficial effects of CDC exosomes: decreased scar mass and improved global function. The increase in viable myocardium does not suffice to increase function, possibly because of inadequate angiogenesis elicited by miR-146a (Halkein et al., 2013). We conclude that miR-146a plays an important part in mediating the effects of CDC exosomes, but alone does not suffice to confer comprehensive therapeutic benefit. Other miRNAs in the repertoire may exert synonymous or perhaps synergistic effects with miR-146a. For instance, miR-22 (another miRNA highly enriched in CDC exosomes) has been shown to be critical for adaptive responses to cardiac stress (Gurha et al., 2012). Likewise, miR-24 (also identified in CDC exosomes) modulates cardiac fibrosis by targeting furin, a member of the profibrotic TGF-β signaling pathway; overexpression of miR-24 in a model of MI decreased myocardial scar formation (Wang et al., 2012). The possible roles of these miRNAs as mediators of CDC exosome benefits, alone or in combination with miR-146a, remain to be studied. Whereas dissection of the active principles within CDC exosomes is worthwhile, deconstruction of the nanovesicles may be counterproductive from a therapeutic perspective. CDC exosomes are naturally cell permeant, and their lipid bilayer coat protects their payloads from degradation as particles shuttle from cell to cell, so that the intact particles themselves may be well suited for disease applications.

Our work implicates exosomes, and the miRNAs they contain, as crucial mediators of CDC-induced cardiac regeneration. CDCs exert diverse but coordinated effects: they recruit endogenous progenitor cells and coax surviving heart cells to proliferate (Chimenti et al., 2010; Li et al., 2010; Malliaras et al., 2013; Stastna et al., 2010); on the other hand, injected CDCs suppress maladaptive LV remodeling (Lee et al., 2011), apoptosis (Cheng et al., 2012; Li et al., 2010), inflammation (Tseliou et al., 2014), and tissue fibrosis (Tseliou et al., 2014) after MI. While it is possible that CDCs secrete a medley of individual growth factors and cytokines that collectively produce diverse benefits, the involvement of master-regulator miRNAs within exosomes would help tie together the various effects without postulating complex mixtures of numerous secreted protein factors. Moreover, miRNAs are known to confer long-lasting benefits and fundamental alterations of the injured microenvironment (Osman, 2012), helping to rationalize the sustained benefits of CDCs despite their evanescent survival in the tissue (Malliaras et al., 2012). CDC exosomes contain rich signaling information conferred by a cell type that is the first shown to be capable of producing regeneration in a setting of "permanent" injury, and confer the same benefits as CDCs without

(D) miR-146a protects stressed neonatal rat cardiomyocytes. Cardiomyocytes were pretreated with 80 nM miR-146a mimic or mimic-control then exposed to 100 μM hydrogen peroxide for 2.5 hr in serum-free media (n = 4 technical replicates; neonatal rat cardiomyocytes under study were derived from 20 to 30 rat pups from three different mothers).
(E) Microarray data showing fold differences in mRNA abundance between miR-146a and mimic-control treated cardiomyocytes. miR-146a suppresses *Irak1* and *Traf6* in stressed neonatal rat cardiomyocytes.
(F) miR-146a-deficient animals have severely impaired cardiac function and structure following acute MI. Pooled data for left ventricular ejection fraction (n = 8 animals per group).
(G–J) Representative Masson's trichrome-stained sections of hearts from three groups (G) and pooled morphometric analysis (H–J; n = 4 hearts per group) reveal impairment of CDC-mediated benefit as evident in pooled data for scar mass, viable mass, and infarct wall thickness (IWT) in hearts injected with GW869-treated CDCs.
*p < 0.05, ¶p < 0.05; **p < 0.01, and ¶¶ p < 0.01 using Student's t test (*KO versus WT; ¶KO versus KO-R). Data are represented as mean and SEM. See also Figures S5 and S6 and Table S1.

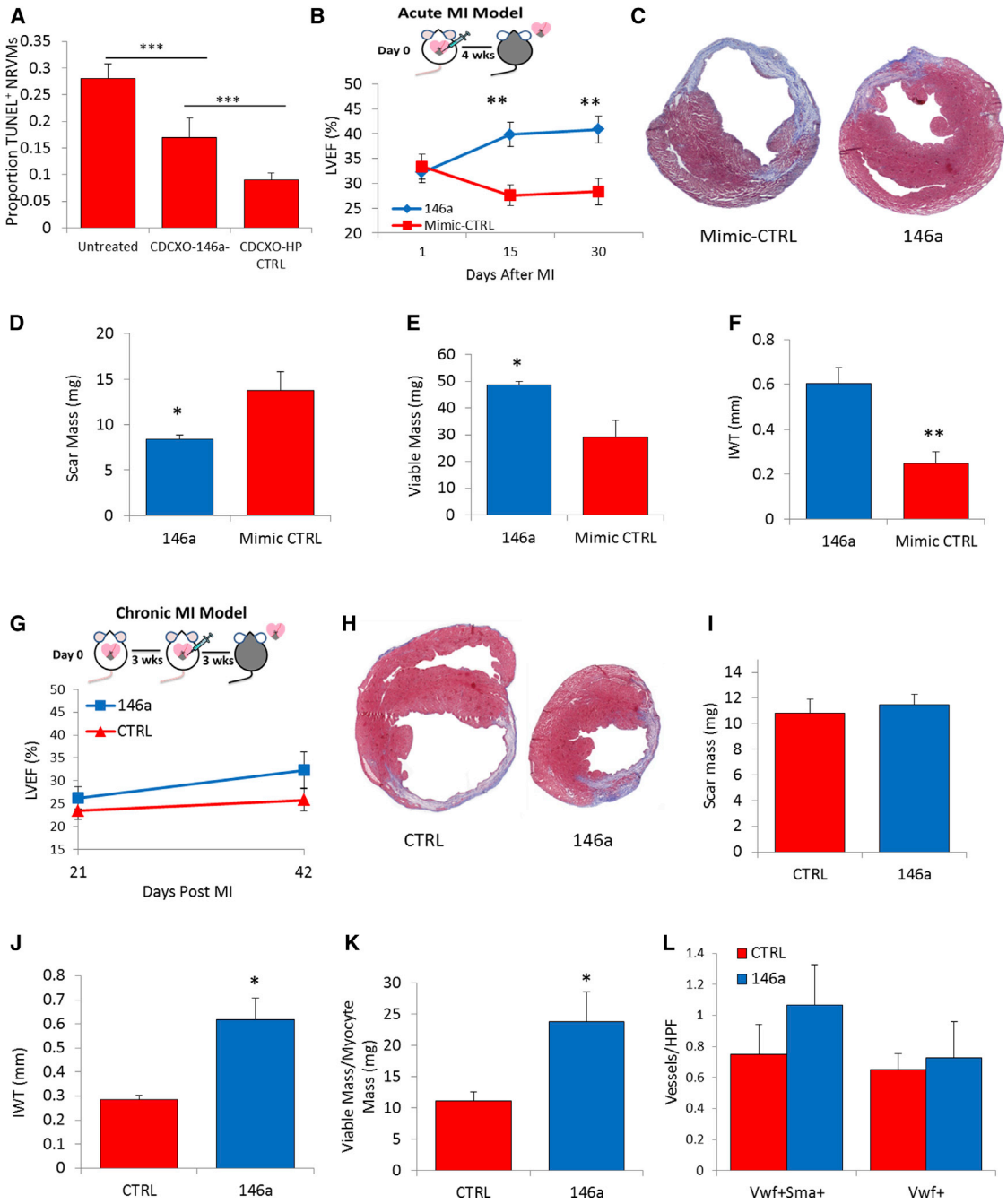

Figure 5. miR-146a Improves Systolic Function in Acute and Chronic Mouse Models of MI

(A) miR-146a knockdown in CDC exosomes diminishes their capacity to protect stressed NRVMs in vitro (n = three technical replicates; neonatal rat cardiomyocytes were derived from 20 to 30 rat pups from three different mothers). CDCs were transfected with either a miR-146a inhibitor or a hairpin control with a sequence based on *Caenorhabditis elegans* microRNAs (HP-CTRL).

(B–F) Acute MI protocol data. Time course of left ventricular ejection fraction (n = 6 animals per group; B). Representative Masson's trichrome-stained sections of hearts from each of the two groups (C) and pooled morphometric analysis (n = 4 hearts per group) reveal decreased scar mass, increased viable mass, and increased infarct wall thickness in animals treated with miR-146a compared to miRNA control (D–F).

(G–L) miR-146a reproduces some of the structural and functional benefits seen in CDC-exosome-treated hearts in a mouse model of chronic MI (miR-146a mimic or mimic control injected on day 21 after MI; n = 6 animals per group). Three weeks later (day 42), animals treated

(legend continued on next page)

transplantation of living cells. For all these reasons, CDC exosomes merit further development as cell-free therapeutic candidates.

EXPERIMENTAL PROCEDURES

Animal Subjects

All procedures related to animals have been conducted under approved Institutional Animal Care and Use Committee protocols.

Human CDC Culture

Endomyocardial biopsies from the right ventricular aspect of the interventricular septum were obtained from healthy hearts of deceased tissue donors. Cardiosphere-derived cells were derived as described previously (Makkar et al., 2012). In brief, heart biopsies were minced into small fragments and briefly digested with collagenase. Explants were then cultured on 20 μg/ml fibronectin (BD biosciences)-coated dishes. Stromal-like flat cells and phase-bright round cells grew out spontaneously from the tissue fragments and reached confluence by 2–3 weeks. These cells were then harvested using 0.25% trypsin (GIBCO) and cultured in suspension on 20 μg/ml poly d-lysine (BD Biosciences) to form self-aggregating cardiospheres. CDCs were obtained by seeding cardiospheres onto fibronectin-coated dishes and passaged. All cultures were maintained at 5% CO_2 at 37°C, using IMDM basic medium (GIBCO) supplemented with 20% FBS (Hyclone), 1% penicillin/streptomycin, and 0.1 ml 2-mercaptoethanol. Human heart biopsy specimens, from which CDCs were grown, were obtained under a protocol approved by the institutional review board for human-subject research.

Media Conditioning and Exosome Purification

Exosomes were harvested from CDCs at passage 4. As a control, we also isolated exosomes from normal human dermal fibroblasts (NHDF). CDCs and NHDFs were conditioned in serum-free media for 15 days at 100% confluence. Media was then centrifuged at 3,000 × *g* for 15 min to remove cellular debris. Exosomes were then isolated using Exoquick ExosomePrecipitation Solution (System Biosciences), which yields high quantities of purified exosomes (Taylor et al., 2011). Exosome pellets were then resuspended in the appropriate media and used for assays. Expression of the conserved exosome marker CD63 was verified using ELISA (System Biosciences). RNA content of exosome pellets was also quantified using a Nanodrop spectrophotometer. For generation of miR-146a-deficient exosomes, CDC were transfected in suspension with miRIDIAN miR-146a hairpin inhibitor or a miRIDIAN hairpin control (Thermo Scientific) and seeded on to fibronectin-coated flasks. Exosomes were isolated from serum-free conditioned media (48 hr conditioning).

Exosomal RNA Degradation

Exosomal RNA degradation was done by suspending exosome pellets in 2 ml of PBS. To one sample, 100 μl of Triton X-100 (Sigma Aldrich) was added to achieve 5% triton concentration. Exosomes were treated with 0.4 μg/ml RNase A treatment for 10 min at 37°C. Samples were further treated with 0.1 mg/ml Proteinase K for 20 min at 37°C. RNA was purified from samples using an miRNA isolation kit (System Biosciences). RNA levels were measured using Nanodrop.

Mass Spectrometry Analysis on Exosome Pellets

Proteins were prepared for digestion using the filter-assisted sample preparation (FASP) method (Wiśniewski et al., 2009). Concentrations were measured using a Qubitfluorometer (Invitrogen). Trypsin was added at a 1:40 enzyme-to-substrate ratio and the sample incubated overnight on a heat block at 37°C. The device was centrifuged and the filtrate collected. Digested peptides were desalted using C_{18} stop-and-go extraction (STAGE) tips (Rappsilber et al., 2003). Peptides were fractionated by strong anion exchange STAGE tip chromatography. Peptides were eluted from the C_{18} STAGE tip and dried. Each fraction was analyzed with liquid chromatography-tandem mass spectrometry. Samples were loaded to a 2 cm × 100 μm I.D. trap column. The analytical column was 13 cm × 75 μm I.D. fused silica with a pulled tip emitter. The mass spectrometer was programmed to acquire, by data-dependent acquisition, tandem mass spectra from the top 15 ions in the full scan from 400 to 1,400 m/z. Mass spectrometer RAW data files were converted to MGF format using msconvert. MGF files were searched using X!Hunter (Craig et al., 2006) against the latest spectral library available on the GPM at the time. MGF files were also searched using X!!Tandem using both the native and k-score (MacLean et al., 2006) scoring algorithms and by OMSSA (Geer et al., 2004). Proteins were required to have one or more unique peptides with peptide E-value scores of 0.01 or less from X!!Tandem, 0.01 or less from OMSSA, 0.001 or less and theta values of 0.5 or greater from X!Hunter searches, and protein E-value scores of 0.0001 or less from X!!Tandem and X!Hunter.

Myocyte Isolation

Neonatal rat cardiomyoctes (NRCMs) were isolated from 1- to 2-day-old Sprague Dawley rat pups and cultured in monolayers as described (Sekar et al., 2009).

Angiogenesis Assay

Human vein umbilical vein endothelial cells were plated on growth factor-deprived Matrigel (BD Biosciences) to assay angiogenesis (Manoussaki et al., 1996). Cells were then incubated with 7 × 10^8 and 4.0 × 10^8 CDC exosomes or NHDF exosomes, respectively. Difference in doses reflects the different exosome output from cells during conditioning. Cells were allowed to

with miR-146a showed comparable cardiac function to control (G) but adverse remodeling was significantly attenuated (H). Scar mass was also similar (I). Viability and infarct wall thickness were significant structural benefits (J and K), but scar mass was not reduced (I). Analysis was done using Student's t test; *p < 0.05, **p < 0.01, and ***p < 0.001. Data are represented as mean and SEM. See also Figures S6 and S7.

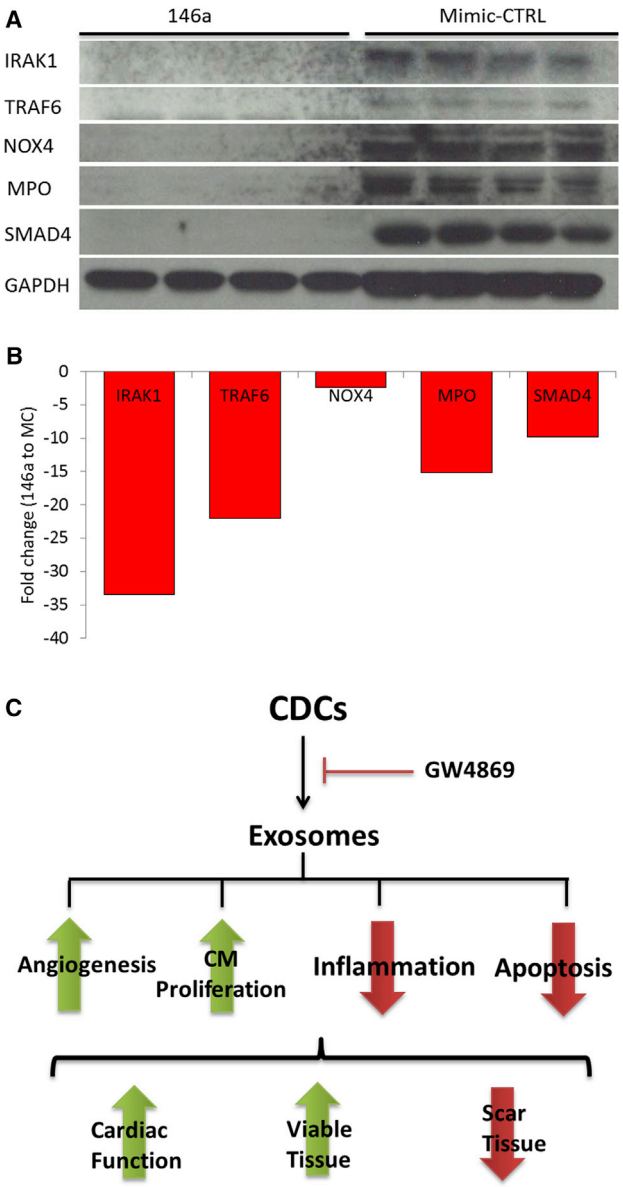

Figure 6. miR-146a Targets Genes Involved in MI Pathology

(A and B) Downregulation of known miR-146a targets in chronic MI mouse hearts 7 days after injection of miR-146a or mimic control. (A) Western blot for IRAK, TRAF6, SMAD4, NOX4, and MPO (a marker of neutrophil infiltration). Each well is loaded with protein lysate pooled from two hearts per group, so that the blot represents pooled samples of two animals each with n = 4 technical replicates. (B) Densitometric analysis of blot in (A) normalized to glyceraldehyde 3-phosphate dehydrogenase (GAPDH).

(C) Schematic of our working hypothesis. CDCs promote functional and structural benefits in the injured myocardium in a primarily paracrine manner. CDCs secrete exosomes that contain miRNAs that mediate benefits in the injured myocardium. These miRNAs target transcripts in the various compartments of the myocardium, which ultimately leads to increased cardiac function, increases in viable tissue, and decrease of scar after MI.

produce exosomes under similar conditions such that the relative doses might be representative of the relative exosome production in vivo. Four hours later, tube formation was measured.

In Vitro Cardiomyocyte Assay

Exosome Treatment

We plated 1.5×10^4 NRCMs in fibronectin-coated eight-chamber slides. After 5 days, media was replaced with new fresh media containing 3.5×10^8 or 2×10^8 CDC or NHDF exosomes, respectively. Cells were then fixed with 4% paraformaldehyde for 30 min at 4°C. Chambers were washed three times with cold PBS then blocked and permeabilized with Dako/0.1% Saponin (Invitrogen) for 1 hr at 37°C. Cells were incubated (overnight, 4°C) with rabbit anti-Ki-67 (1:100) primary antibody and mouse anti-α-sarcomeri-cactinin (Abcam). Cells were then washed three times with PBS and incubated with goat antimouse (Cy5) and goat antirabbit (FITC) in TUNEL stain solution for 1 hr at 37°C. Slides were then washed three times in PBS, stained with 1:8,000 4′,6-diamidino-2-phenylindole stain solution, and mounted using Prolong antifade solution(Invitrogen). Slides were imaged using confocal microscopy.

Cardiomyocyte Stress Assay

NRCMs were plated in a monolayer on fibronectin-coated 12-well plates and treated with either 40 nM of miR-146a or mimic for 24 hr. Media was then changed and cells were washed three times with PBS. Cells were then stressed using of hydrogen peroxide (100 μM H_2O_2 in serum free media for 2 hr) or cobalt chloride (5 mM $CoCl_2$ in serum-free media for 2 hr). Viability was measured by washing cells with PBS and treating with 20 μM Calcein PBS solution for 20 min at 37°C in dark conditions. Fluorescence was read using a Soft Max Pro 5 Plate Reader (Molecular Devices). Data per well is the average of nine consecutive measurements. A second model used in this study involved plating cardiomyocytes on 25 mm precoated glass coverslips (Fischer Scientific) in six-well plates. Cells were stressed using 50 μM H_2O_2 for 15 min followed incubation with transwell membrane inserts containing CDCs or incubation with CDC exosomes for 4 hr. Cells were then washed, fixed with paraformaldehyde, and stained for analysis as explained above.

Exosome Inhibition in CDCs

CDCs were grown to confluence in T175 flasks. For in vitro studies, CDCs were conditioned for 15 days in 20 μM GW4869 (Sigma Aldrich), serum-free media, or serum-free media containing an equivalent volume of DMSO. For in vitro transwell insert assays of cardiomyocyte stress, we treated CDCs with 20 μM GW4869 (Sigma Aldrich), or 5 μM Spiroepoxide (Santa Cruz Biotechnology) for 12 hr. CDCs were then washed three times in PBS and supplanted with serum-free media. Inserts containing treated CDCs were then added into six-well plates containing cardiomyocytes. For in vivo studies, CDCs were treated with 20 μM GW4869 or an equivalent volume of DMSO for 12 hr. Prior to injection, CDC flasks were washed twice with PBS, trypsinized, and counted; 10^5 CDCs were injected per animal.

Acute and Chronic Myocardial Infarction Model

Three-month-old male severe combined immunodeficient (SCID)-beige mice were anesthetized with isoflurane. Following surgical

preparation, a 2 cm vertical incision was performed in the midclavicular line for a lateral thoracotomy. The left anterior descending was ligated using 7-0 silk. Animals were injected with exosomes, miRNAs, CDCs, or media control at two peri-infarct sites with a volume of 40 μl per injection (Smith et al., 2007). For the chronic model of MI, animals were infarcted as described above without any treatment administration. Three weeks later, the animals were given the treatment in the same manner as above. For exosome treatments, pellets were resuspended in Iscove's Modified Dulbecco's (IMDM) basal media. Animals were injected with 2.8×10^9 and 1.56×10^9 of CDC and NHDF exosomes, respectively. miRNA-treated animals were injected with 80 ng of miR-146a or miRNA mimic control. In brief, miRIDIAN miR-146a or miRIDIAN negative control (Thermo Scientific) was vortexed in Dharmafect (Thermo Scientific) transfection reagent and IMDM basal media and incubated for 10 min at room temperature to allow complexes to form. miRNA complexes were then resuspended in IMDM for injection. For CDC treatments, animals were injected with 10^5 CDCs as described (Li et al., 2012).

Echocardiography

SCID beige mice underwent echocardiography 24 hr (baseline), 14 days, and 4 weeks after surgery using Vevo 770 Imaging System (Visual Sonics) (Smith et al., 2007). After induction of light general anesthesia, hearts were 3D imaged in the long axis view at the level of maximum left ventricular diameter. Left ventricular ejection fraction was measured with Visual Sonics version 1.3.8 software from 2D views of LV end-diastolic and LV end-systolic area. Each animal/time point was measured multiple times and the average was used for statistical analysis.

Histology

Animals were sacrificed 4 weeks after MI. Hearts were harvested and a transverse cut was made slightly above the MI suture. The apical portion was then imbedded in optimum cutting temperature solution in a base mold/embedding ring block (Tissue Tek). Blocks were immediately frozen by submersion in cold 2-methylbutane. Hearts were sectioned at a thickness of 5 μM.

Masson's Trichrome Staining

Two slides containing a total of four sections per heart were stained using Masson's trichrome stain. In brief, sections were treated overnight in Bouin's solution. Slides were then rinsed for 10 min under running water and stained with Weigert's hematoxylin for 5 min. Slides were then rinsed and stained with scarlet-acid fuchsin for 5 min and rinsed again. Slides were then stained with phosphotungstic/phosphomolybdic, aniline blue, and 2% acetic acid for 5 min each. Slides were then rinsed, dried, and mounted using DPX mounting media.

Morphometry

Morphometric analysis of heart sections was performed using Image J software (Makkar et al., 2012). In brief, 2D images of stained sections were split into blue, red, and green channels (only the blue was used). Infarct size was made by measuring area and intensity of blue in each section to calculate infarct size. Percent viable and infarct mass were calculated by averaging percent infarct across four sections analyzed per heart. Infarct and viable masses were calculated as the product of the infarct or viable tissue, the height of the average mouse heart (3 mm) and the specific gravity of heart tissue (1.05 g/ml). Infarct wall thickness was calculated by measuring the thinnest area of the infarct. In the chronic model of MI where significant hypertrophy and adverse remodeling took place, we adjusted the viable mass of each heart based on the derived mass of cardiomyocytes in the tissue. Myocyte mass was obtained by measuring the cross-sectional area of perpendicularly sectioned cardiomyocytes (defined as round cells with red cytoplasm and a visible nucleus in the center). We measured at least 25 myocytes per heart. Myocyte volume was quantified using the simplifying assumption of a cylindrical shape; mass was derived by multiplying volumes by the specific gravity of a cardiomyocyte (1.15 mg/μl). The viable mass of each mouse heart was divided by the mass of the cardiomyocytes in that heart.

SUPPLEMENTAL INFORMATION

Supplemental Information includes Supplemental Discussion, seven figures, and one table and can be found with this article online at http://dx.doi.org/10.1016/j.stemcr.2014.04.006.

ACKNOWLEDGMENTS

We thank Baiming Sun for performing animal surgeries, Geoffrey De Couto for advice on the apoptosis assays, Susmita Sahoo for helpful discussions regarding the experimental protocol used in Figure 1B, and Ryan Middleton and Weixin Liu for technical assistance. This work was supported by a grant from the NIH to E.M. E.M. is founder of, unpaid advisor to, and owns equity in Capricor Therapeutics.

Received: January 2, 2014
Revised: April 8, 2014
Accepted: April 9, 2014
Published: May 6, 2014

REFERENCES

Arroyo, J.D., Chevillet, J.R., Kroh, E.M., Ruf, I.K., Pritchard, C.C., Gibson, D.F., Mitchell, P.S., Bennett, C.F., Pogosova-Agadjanyan, E.L., Stirewalt, D.L., et al. (2011). Argonaute2 complexes carry a population of circulating microRNAs independent of vesicles in human plasma. Proc. Natl. Acad. Sci. USA *108*, 5003–5008.

Arslan, F., Smeets, M.B., O'Neill, L.A., Keogh, B., McGuirk, P., Timmers, L., Tersteeg, C., Hoefer, I.E., Doevendans, P.A., Pasterkamp, G., and de Kleijn, D.P. (2010). Myocardial ischemia/reperfusion injury is mediated by leukocytic toll-like receptor-2 and reduced by systemic administration of a novel anti-toll-like receptor-2 antibody. Circulation *121*, 80–90.

Arslan, F., Lai, R.C., Smeets, M.B., Akeroyd, L., Choo, A., Aguor, E.N., Timmers, L., van Rijen, H.V., Doevendans, P.A., Pasterkamp, G., et al. (2013). Mesenchymal stem cell-derived exosomes increase ATP levels, decrease oxidative stress and activate PI3K/Akt pathway to enhance myocardial viability and prevent adverse remodeling after myocardial ischemia/reperfusion injury. Stem Cell Res. (Amst.) *10*, 301–312.

Cheng, K., Malliaras, K., Li, T.S., Sun, B., Houde, C., Galang, G., Smith, J., Matsushita, N., and Marbán, E. (2012). Magnetic enhancement of cell retention, engraftment, and functional benefit after intracoronary delivery of cardiac-derived stem cells in a rat model of ischemia/reperfusion. Cell Transplant. *21*, 1121–1135.

Cheng, H.S., Sivachandran, N., Lau, A., Boudreau, E., Zhao, J.L., Baltimore, D., Delgado-Olguin, P., Cybulsky, M.I., and Fish, J.E. (2013). MicroRNA-146 represses endothelial activation by inhibiting pro-inflammatory pathways. EMBO Mol Med *5*, 949–966.

Cheng, K., Malliaras, K., Smith, R.R., Shen, D., Sun, B., Blusztajn, A., Xie, Y., Ibrahim, A., Aminzadeh, M.A., Liu, W., et al. (2014). Human Cardiosphere-Derived Cells From Advanced Heart Failure Patients Exhibit Augmented Functional Potency in Myocardial Repair. JACC Heart Fail *2*, 49–61.

Chimenti, I., Smith, R.R., Li, T.S., Gerstenblith, G., Messina, E., Giacomello, A., and Marbán, E. (2010). Relative roles of direct regeneration versus paracrine effects of human cardiosphere-derived cells transplanted into infarcted mice. Circ. Res. *106*, 971–980.

Craig, R., Cortens, J.C., Fenyo, D., and Beavis, R.C. (2006). Using annotated peptide mass spectrum libraries for protein identification. J. Proteome Res. *5*, 1843–1849.

Denzer, K., Kleijmeer, M.J., Heijnen, H.F., Stoorvogel, W., and Geuze, H.J. (2000). Exosome: from internal vesicle of the multivesicular body to intercellular signaling device. J. Cell Sci. *113*, 3365–3374.

Feng, Y., Zhao, H., Xu, X., Buys, E.S., Raher, M.J., Bopassa, J.C., Thibault, H., Scherrer-Crosbie, M., Schmidt, U., and Chao, W. (2008). Innate immune adaptor MyD88 mediates neutrophil recruitment and myocardial injury after ischemia-reperfusion in mice. Am. J. Physiol. Heart Circ. Physiol. *295*, H1311–H1318.

Geer, L.Y., Markey, S.P., Kowalak, J.A., Wagner, L., Xu, M., Maynard, D.M., Yang, X., Shi, W., and Bryant, S.H. (2004). Open mass spectrometry search algorithm. J. Proteome Res. *3*, 958–964.

Gurha, P., Abreu-Goodger, C., Wang, T., Ramirez, M.O., Drumond, A.L., van Dongen, S., Chen, Y., Bartonicek, N., Enright, A.J., Lee, B., et al. (2012). Targeted deletion of microRNA-22 promotes stress-induced cardiac dilation and contractile dysfunction. Circulation *125*, 2751–2761.

Halkein, J., Tabruyn, S.P., Ricke-Hoch, M., Haghikia, A., Nguyen, N.Q., Scherr, M., Castermans, K., Malvaux, L., Lambert, V., Thiry, M., et al. (2013). MicroRNA-146a is a therapeutic target and biomarker for peripartum cardiomyopathy. J. Clin. Invest. *123*, 2143–2154.

Hergenreider, E., Heydt, S., Tréguer, K., Boettger, T., Horrevoets, A.J., Zeiher, A.M., Scheffer, M.P., Frangakis, A.S., Yin, X., Mayr, M., et al. (2012). Atheroprotective communication between endothelial cells and smooth muscle cells through miRNAs. Nat. Cell Biol. *14*, 249–256.

Huang, Y., Crawford, M., Higuita-Castro, N., Nana-Sinkam, P., and Ghadiali, S.N. (2012). miR-146a regulates mechanotransduction and pressure-induced inflammation in small airway epithelium. FASEB J. *26*, 3351–3364.

Infanger, D.W., Cao, X., Butler, S.D., Burmeister, M.A., Zhou, Y., Stupinski, J.A., Sharma, R.V., and Davisson, R.L. (2010). Silencing nox4 in the paraventricular nucleus improves myocardial infarction-induced cardiac dysfunction by attenuating sympathoexcitation and periinfarct apoptosis. Circ. Res. *106*, 1763–1774.

Johnstone, R.M. (2005). Revisiting the road to the discovery of exosomes. Blood Cells Mol. Dis. *34*, 214–219.

Kosaka, N., Iguchi, H., Yoshioka, Y., Takeshita, F., Matsuki, Y., and Ochiya, T. (2010). Secretory mechanisms and intercellular transfer of microRNAs in living cells. J. Biol. Chem. *285*, 17442–17452.

Kreke, M., Smith, R.R., Marbán, L., and Marbán, E. (2012). Cardiospheres and cardiosphere-derived cells as therapeutic agents following myocardial infarction. Expert Rev. Cardiovasc. Ther. *10*, 1185–1194.

Lee, S.T., White, A.J., Matsushita, S., Malliaras, K., Steenbergen, C., Zhang, Y., Li, T.S., Terrovitis, J., Yee, K., Simsir, S., et al. (2011). Intramyocardial injection of autologous cardiospheres or cardiosphere-derived cells preserves function and minimizes adverse ventricular remodeling in pigs with heart failure post-myocardial infarction. J. Am. Coll. Cardiol. *57*, 455–465.

Li, T.S., Cheng, K., Lee, S.T., Matsushita, S., Davis, D., Malliaras, K., Zhang, Y., Matsushita, N., Smith, R.R., and Marbán, E. (2010). Cardiospheres recapitulate a niche-like microenvironment rich in stemness and cell-matrix interactions, rationalizing their enhanced functional potency for myocardial repair. Stem Cells *28*, 2088–2098.

Li, T.S., Cheng, K., Malliaras, K., Smith, R.R., Zhang, Y., Sun, B., Matsushita, N., Blusztajn, A., Terrovitis, J., Kusuoka, H., et al. (2012). Direct comparison of different stem cell types and subpopulations reveals superior paracrine potency and myocardial repair efficacy with cardiosphere-derived cells. J. Am. Coll. Cardiol. *59*, 942–953.

Liu, Z., Lu, C.L., Cui, L.P., Hu, Y.L., Yu, Q., Jiang, Y., Ma, T., Jiao, D.K., Wang, D., and Jia, C.Y. (2012). MicroRNA-146a modulates TGF-β1-induced phenotypic differentiation in human dermal fibroblasts by targeting SMAD4. Arch. Dermatol. Res. *304*, 195–202.

Lugini, L., Cecchetti, S., Huber, V., Luciani, F., Macchia, G., Spadaro, F., Paris, L., Abalsamo, L., Colone, M., Molinari, A., et al. (2012). Immune surveillance properties of human NK cell-derived exosomes. J. Immunol. *189*, 2833–2842.

MacLean, B., Eng, J.K., Beavis, R.C., and McIntosh, M. (2006). General framework for developing and evaluating database scoring algorithms using the TANDEM search engine. Bioinformatics *22*, 2830–2832.

Makkar, R.R., Smith, R.R., Cheng, K., Malliaras, K., Thomson, L.E., Berman, D., Czer, L.S., Marbán, L., Mendizabal, A., Johnston, P.V., et al. (2012). Intracoronary cardiosphere-derived cells for heart regeneration after myocardial infarction (CADUCEUS): a prospective, randomised phase 1 trial. Lancet *379*, 895–904.

Malliaras, K., Li, T.S., Luthringer, D., Terrovitis, J., Cheng, K., Chakravarty, T., Galang, G., Zhang, Y., Schoenhoff, F., Van Eyk, J., et al. (2012). Safety and efficacy of allogeneic cell therapy in infarcted rats transplanted with mismatched cardiosphere-derived cells. Circulation *125*, 100–112.

Malliaras, K., Zhang, Y., Seinfeld, J., Galang, G., Tseliou, E., Cheng, K., Sun, B., Aminzadeh, M., and Marbán, E. (2013). Cardiomyocyte proliferation and progenitor cell recruitment underlie therapeutic

regeneration after myocardial infarction in the adult mouse heart. EMBO Mol Med *5*, 191–209.

Manoussaki, D., Lubkin, S.R., Vernon, R.B., and Murray, J.D. (1996). A mechanical model for the formation of vascular networks in vitro. Acta Biotheor. *44*, 271–282.

O'Loughlin, A.J., Woffindale, C.A., and Wood, M.J. (2012). Exosomes and the emerging field of exosome-based gene therapy. Curr. Gene Ther. *12*, 262–274.

Osman, A. (2012). MicroRNAs in health and disease—basic science and clinical applications. Clin. Lab. *58*, 393–402.

Oyama, J., Blais, C., Jr., Liu, X., Pu, M., Kobzik, L., Kelly, R.A., and Bourcier, T. (2004). Reduced myocardial ischemia-reperfusion injury in toll-like receptor 4-deficient mice. Circulation *109*, 784–789.

Pan, B.T., and Johnstone, R.M. (1983). Fate of the transferrin receptor during maturation of sheep reticulocytes in vitro: selective externalization of the receptor. Cell *33*, 967–978.

Pan, B.T., Teng, K., Wu, C., Adam, M., and Johnstone, R.M. (1985). Electron microscopic evidence for externalization of the transferrin receptor in vesicular form in sheep reticulocytes. J. Cell Biol. *101*, 942–948.

Rappsilber, J., Ishihama, Y., and Mann, M. (2003). Stop and go extraction tips for matrix-assisted laser desorption/ionization, nanoelectrospray, and LC/MS sample pretreatment in proteomics. Anal. Chem. *75*, 663–670.

Sahoo, S., Klychko, E., Thorne, T., Misener, S., Schultz, K.M., Millay, M., Ito, A., Liu, T., Kamide, C., Agrawal, H., et al. (2011). Exosomes from human CD34(+) stem cells mediate their proangiogenic paracrine activity. Circ. Res. *109*, 724–728.

Sekar, R.B., Kizana, E., Cho, H.C., Molitoris, J.M., Hesketh, G.G., Eaton, B.P., Marbán, E., and Tung, L. (2009). IK1 heterogeneity affects genesis and stability of spiral waves in cardiac myocyte monolayers. Circ. Res. *104*, 355–364.

Singh, M.V., Swaminathan, P.D., Luczak, E.D., Kutschke, W., Weiss, R.M., and Anderson, M.E. (2012a). MyD88 mediated inflammatory signaling leads to CaMKII oxidation, cardiac hypertrophy and death after myocardial infarction. J. Mol. Cell. Cardiol. *52*, 1135–1144.

Singh, P.P., Smith, V.L., Karakousis, P.C., and Schorey, J.S. (2012b). Exosomes isolated from mycobacteria-infected mice or cultured macrophages can recruit and activate immune cells in vitro and in vivo. J. Immunol. *189*, 777–785.

Smith, R.R., Barile, L., Cho, H.C., Leppo, M.K., Hare, J.M., Messina, E., Giacomello, A., Abraham, M.R., and Marbán, E. (2007). Regenerative potential of cardiosphere-derived cells expanded from percutaneous endomyocardial biopsy specimens. Circulation *115*, 896–908.

Stastna, M., Chimenti, I., Marbán, E., and Van Eyk, J.E. (2010). Identification and functionality of proteomes secreted by rat cardiac stem cells and neonatal cardiomyocytes. Proteomics *10*, 245–253.

Taylor, D.D., Zacharias, W., and Gercel-Taylor, C. (2011). Exosome isolation for proteomic analyses and RNA profiling. Methods Mol. Biol. *728*, 235–246.

Thomas, S., and Bonchev, D. (2010). A survey of current software for network analysis in molecular biology. Hum. Genomics *4*, 353–360.

Trajkovic, K., Hsu, C., Chiantia, S., Rajendran, L., Wenzel, D., Wieland, F., Schwille, P., Brügger, B., and Simons, M. (2008). Ceramide triggers budding of exosome vesicles into multivesicular endosomes. Science *319*, 1244–1247.

Tseliou, E., de Couto, G., Terrovitis, J., Sun, B., Weixin, L., Marbán, L., and Marbán, E. (2014). Angiogenesis, cardiomyocyte proliferation and anti-fibrotic effects underlie structural preservation post-infarction by intramyocardially-injected cardiospheres. PLoS ONE *9*, e88590.

Vasa-Nicotera, M., Chen, H., Tucci, P., Yang, A.L., Saintigny, G., Menghini, R., Mahè, C., Agostini, M., Knight, R.A., Melino, G., and Federici, M. (2011). miR-146a is modulated in human endothelial cell with aging. Atherosclerosis *217*, 326–330.

Virag, J.I., and Murry, C.E. (2003). Myofibroblast and endothelial cell proliferation during murine myocardial infarct repair. Am. J. Pathol. *163*, 2433–2440.

Wang, J., Huang, W., Xu, R., Nie, Y., Cao, X., Meng, J., Xu, X., Hu, S., and Zheng, Z. (2012). MicroRNA-24 regulates cardiac fibrosis after myocardial infarction. J. Cell. Mol. Med. *16*, 2150–2160.

Wang, X., Ha, T., Liu, L., Zou, J., Zhang, X., Kalbfleisch, J., Gao, X., Williams, D., and Li, C. (2013). Increased expression of microRNA-146a decreases myocardial ischaemia/reperfusion injury. Cardiovasc. Res. *97*, 432–442.

Wiśniewski, J.R., Zougman, A., Nagaraj, N., and Mann, M. (2009). Universal sample preparation method for proteome analysis. Nat. Methods *6*, 359–362.

Zhu, H., and Fan, G.C. (2011). Extracellular/circulating microRNAs and their potential role in cardiovascular disease. Am J Cardiovasc Dis *1*, 138–149.